Bulletin of the Seismological Society of America, Vol. 106, No. 5, pp. 1939–1947, October 2016, doi: 10.1785/0120160058

Coda Q in the Northern Cascadia Subduction Zone

by Amir Mansour Farahbod, Andrew J. Calvert, John F. Cassidy, and Camille Brillon

Abstract Using seismograms recorded at 66 Canadian seismic stations, coda Q was estimated from earthquakes in southwestern British Columbia and northern Washington State, employing the single backscattering approximation. A total of 580 earthquakes with magnitudes ranging from 1.2 to 6.4, depths from 0 to 67 km, and epicentral distances of 5–110 km were selected to obtain 3022 high signal-to-noise ratio traces for analysis. An average of all the data yields a relationship for coda Q of $Q_C = 72f^{0.91}$. There is little variation of this coda Q relationship when using either crustal or in-slab sources, which represent uniform sampling of the crust and upper mantle. Crustal earthquakes result in a relationship of $Q_C = 73f^{0.89}$, and for in-slab events Q_C can be expressed as $Q_C = 69f^{0.94}$. In general, Q_0 (Q_C at 1 Hz) increases from the west coast of Vancouver Island to the east-southeast within the Coast belt. Stations on west-central Vancouver Island closest to the landward projection of the Nootka fault zone, and the location of the only two known large crustal earthquakes (1918 $\mathbf{M} \sim 7$ and 1946 $\mathbf{M} \sim 7.3$) on Vancouver Island, have the lowest Q_0 values in our study area, suggesting a contrast in Q between the north and south of the island.

Online Material: Figure showing principal tectonic units and station locations, and tables of average Q_0 and alpha values with estimated uncertainties.

Introduction

Attenuation of seismic waves during propagation, which is typically described in terms of the seismic quality factor Q, is an important characteristic of Earth structure. This effect, which is due to conversion of elastic energy to heat or other forms of energy (intrinsic attenuation), as well as energy redistribution (scattering) in a heterogeneous medium (Wu and Aki, 1988; Mak *et al.*, 2004), is proportional to Q^{-1}. The relative contribution of the scattering attenuation and intrinsic absorption varies from region to region and also depends on frequency (Jin and Aki, 2005). A strong correlation between coda Q, or Q_C, and seismicity has been reported in both space (Jin and Aki, 1988) and time (Jin and Aki, 1989). Coda Q also varies systematically by more than one order of magnitude with the degree of recent tectonic activity (Mitchell and Cong, 1998; Sato and Fehler, 1998). However, most maps of coda Q have low-spatial resolution because of the large station spacing and the use of relatively distant earthquakes (Jin and Aki, 2005).

In southwestern British Columbia and northern Washington State (Fig. 1), which is an active subduction zone and has a diverse tectonic environment, well-distributed seismograph networks provide a good data set to study the spatial variation of coda Q. Early (and limited) coda Q studies in this region (Havskov *et al.*, 1989; Zelt *et al.*, 1999) indicated that, similar to other tectonically active areas, northern Cascadia is associated with low Q_0 (Q_C at 1 Hz) values. However, at the time of those studies, the limited data and uneven distribution of earthquakes were two main barriers to the construction of a robust regional picture of coda Q. In this study, we significantly expanded the earthquake database by including all available waveforms, which were recorded by temporary and permanent seismic stations in the region over a 30-year period (1985–2015), to calculate the coda decay rates of local earthquakes. As a result, we greatly improved the reliability and resolution of the coda Q estimates across northern Cascadia by increasing the number of events and introducing measurements at smaller source–station distances.

Methodology

We determine the coda Q, or Q_C, using the single backscattering approximation, which assumes that the S coda waves comprise secondary S waves produced by heterogeneities inside the propagation medium (Aki, 1969; Aki and Chouet, 1975). The coda-wave amplitude A at frequency f and lapse time t (time from the event origin) is described by

$$A(f,t) = S(f)t^{-\beta}e^{-\pi f t/Q_c}, \tag{1}$$

in which $S(f)$ is the source factor, which is related to the earthquake source spectrum and includes station site, back-

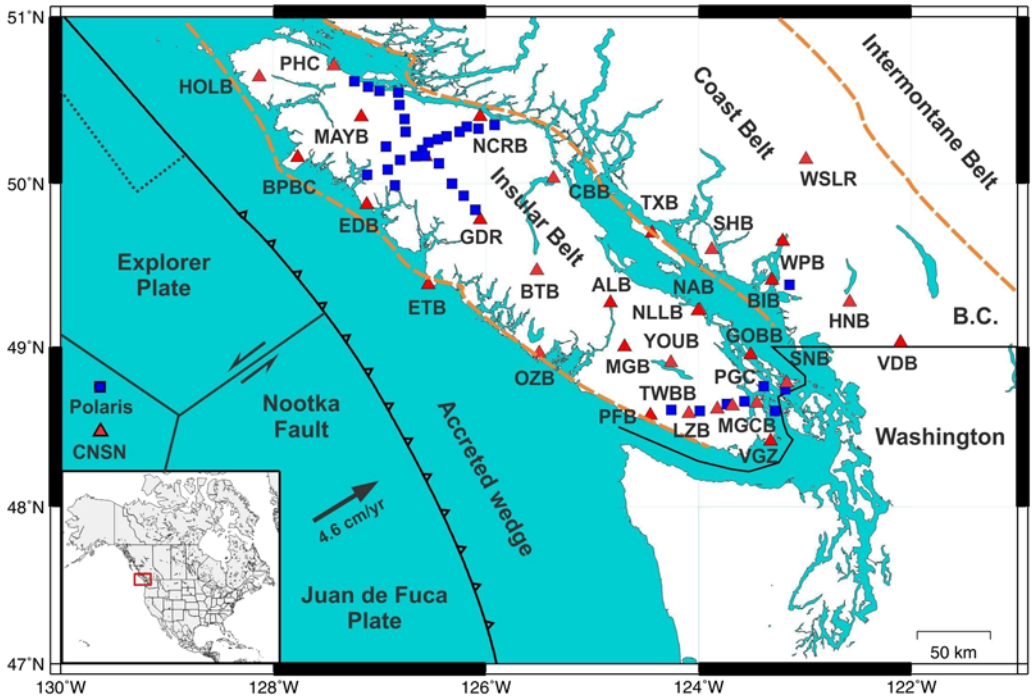

Figure 1. Principal tectonic units (boundaries are denoted by dashed lines) and seismograph stations in the study area in southwestern British Columbia from which the waveform data for this study were obtained. Triangles with station code indicate Canadian National Seismic Network (CNSN) broadband and short-period stations and squares are Portable Observatories for Lithospheric Analysis and Research Investigating Seismicity (POLARIS) broadband seismograph stations. (Inset) Location map of the study area in North America. The color version of this figure is available only in the electronic edition.

scattering, and source effects (Wu and Aki, 1988), and β is a geometrical spreading parameter. Equation (1) assumes that the source and receiver are at the same point, which is only a good approximation for signals at a lapse time t, greater than twice the S-wave travel time t_S (Sato, 1977; Rautian and Khalturin, 1978). For body waves (this study) $\beta = 1$ and equation (1) can be written as

$$\ln(A(f,t)) + \ln(t) = \ln(S(f)) - \pi f t/Q_C. \qquad (2)$$

Plotting the envelope of $\ln(A(f,t)) + \ln(t)$ as a function of t for a given frequency (by band-pass filtering the signal), gives a straight line with slope $-\pi f/Q_C$, and Q_C can be determined (Havskov and Ottemöller, 2010). By calculating the Q_C values for different frequencies, the frequency dependence of this quantity can be expressed as $Q_C = Q_0 f^{\alpha}$ (Rautian and Khalturin, 1978), with Q_0 and α obtained by linear regression of $\log(Q_C)$ on $\log(f)$.

The volume sampled by the backscattered waves is one-half of a 3D ellipsoid with the source and receiver as focal points; the semimajor axis $a_1 = V_S t/2$ and semiminor axis $a_2 = (a_1^2 – R^2/4)^{1/2}$, in which V_S is the average S-wave velocity (3.5 km/s) and R is the station-event separation (Pauli, 1984; Zelt *et al.*, 1999). For similar a_1 and a_2, the sampled volume is nearly a sphere, and the maximum depth sampled is approximately given by $Z_{\max} = a_2 + d/2$, in which d is the event depth (Havskov *et al.*, 1989; Zelt *et al.*, 1999).

Estimates of coda Q are quite sensitive to selection of parameters such as window length, lapse time, minimum correlation coefficient, and filter band width. It is therefore important when comparing coda Q results from different studies that the processing parameters are known and ideally identical (Havskov and Ottemöller, 2010; Havskov *et al.*, 2016). Several studies show an increase in Q_C with increasing lapse time, which likely is a result of including a greater volume of less-complex upper-mantle material in the sampling volume (Pauli, 1984; Gusev, 1995; Zelt *et al.*, 1999). When the lapse time increases, almost all studies find increased Q_C and conclude that the longer lapse times mean that deeper, high Q_C areas are sampled (Havskov and Ottemöller, 2010).

Data and Analysis

To calculate coda Q, we used waveform data from 66 seismograph stations of the Geological Survey of Canada (GSC) and Portable Observatories for Lithospheric Analysis and Research Investigating Seismicity (POLARIS) networks, which have flat frequency responses from 1 to 16 Hz. The GSC network is composed of permanent stations equipped with broadband and/or short-period sensors, and records are sampled at the rate of either 100 or 40 samples per second. On the other hand, POLARIS is a temporary network of broadband stations that was periodically deployed to different regions of Canada from 2000 to 2014.

In this study, nine stations are located in the Coast belt, a suture zone between the Intermontaine belt and Insular belt

(Fig. 1). The formation of the Coast belt, which is composed of plutonic and metamorphic rock, was initiated by the collision of the Insular superterrane with the western margin of North America in the mid-Cretaceous through early Cenozoic time (Monger and Price, 2002). The remaining seismograph stations are located on the Insular belt, which comprises sedimentary and volcanic rocks deposited from the Paleozoic to Mesozoic time. All of these stations fall within the active northern Cascadia subduction zone.

For each event–station pair, we picked *P*-wave and *S*-wave arrivals and relocated earthquakes with $V_P/V_S = 1.76$ (A. M. Farahbod and A. J. Calvert, unpublished data, 2007; see Data and Resources) and then calculated Q_C at five frequencies between 2 and 16 Hz using equation (2). For each station, Q_C is determined by averaging the calculated values from all events. The dataset comprises 580 events recorded between 1985 and 2015 with magnitudes ranging from 1.2 to 6.4, depths from 0 to 67 km, and distances of ~5 to ~110 km (Fig. 2). This gives a total of 3022 high signal-to-noise ratio (SNR) traces ≥ 5.0 (SNR is calculated using the last seconds of the filtered coda window and the first seconds of the noise window in front of the signal); however, the number of traces actually used for analysis depends on sampling size. The coda window length used in this study is 20 s, and results with correlation coefficients less than 0.5 (for the fit of equation 2) were considered poor fits and were rejected.

We used the computer program SEISAN (Havskov and Ottemöller, 2012) to calculate coda Q. The program calculates Q_C for a series of events and stations at five frequencies (2, 4, 8, 12, and 16 Hz). On completion, the average value for each frequency is calculated, and Q_C versus f curve is fitted to the average values (Havskov and Ottemöller, 2012). The program also plots the individual events and filtered coda windows (e.g., Fig. 3).

Results

We computed Q_C across the northern Cascadia subduction zone for a total number of 580 earthquakes recorded at 66 seismic stations. Our results (average Q_0 and average alpha values for a range of ellipse parameter a_2, from 40 to 100 km), with five or more events used for each estimate, are summarized in Tables 1 and 2, and in Figure 4. Less reliable estimates (with the number of events for each average value between 2 and 4) and also our results corresponding to ellipse parameter a_2 of 30 km are listed in Ⓔ Tables S1–S2, and S3 (available in the electronic supplement to this article), respectively. Solutions based on one event only are not considered in this study. The total number of coda Q determinations at any frequency is 4641, which on average represents eight estimates per event, similar to many attenuation studies around the globe (Havskov *et al.*, 2016). Our results for one station (BBB) in the northern tip of the Cascadia subduction zone (see Ⓔ Fig. S1) and also the only available Q_0 estimates for three closed stations in southwestern British Columbia (Zelt *et al.*, 1999) are presented in Ⓔ Table S4.

We examined (Fig. 2) both crustal earthquakes (288 events and 3497 measurements at frequencies from 2 to 16 Hz) and in-slab earthquakes (4979 measurements at frequencies from 2 to 16 Hz) using high (≥5) SNR events. We find little difference in the coda Q relationship when using crustal or in-slab sources, which represent a fairly uniform sampling of the crust and upper mantle across the northern Cascadia subduction zone. Crustal earthquakes yield a Q relationship of $Q_C = 73f^{0.89}$, and for in-slab events coda Q can be expressed as $Q_C = 69f^{0.94}$. An average over the crustal and in-slab earthquakes gives a relationship of $Q_C = 72f^{0.91}$ for frequencies in the 2–16 Hz range. This represents a lower Q_0 and higher α than the corresponding previous estimates for southwestern British Columbia ($Q_C = 110f^{0.72}$; Zelt *et al.*, 1999) and higher Q_0 and lower α in comparison with results for northern Washington State ($Q_C = 63f^{0.97}$; Havskov *et al.*, 1989), with maximum source–station separation in both studies of ~70 km. We note, however, that our results are based on a much larger data set composed of 3022 high SNR traces, compared with 206 traces used in the Havskov *et al.* (1989) Washington state study, and 145 traces used in the Zelt *et al.* (1999) southwest British Columbia study.

In general, Q_0 values allow a quantitative comparison from station to station and with other studies and are generally indicative of the tectonic nature of the regions. Therefore, we calculated the Q_0 values for each station for several sampling volumes with average ellipse parameter of a_2 between 40 and 100 km (Fig. 4). The corresponding estimated Q_0 error for each station with five or more events ranges from 4 to 20 (Table 1). The average of maximum depth sampled at different stations ranges from 50 to 112 km (Table 2), with an overall average of 83 km. Q_C is plotted as a function of frequency (and for different sampling volumes) for the average of all stations in Figure 5. Overall there is an increase in Q_0 values with increasing sampling volume.

Our estimated Q_0 values are lowest along the west coast of Vancouver Island (Figs. 4 and 5) and highest in the Coast belt (consistent with the overall observations of Zelt *et al.*, 1999). The lowest Q_0 value of 44 was found at station ETB with ellipse parameter a_2 of 50 km, and the lowest α value of 0.67 was found at station WPB with $a_2 = 100$ km (Tables 1 and 2). Q_0 is consistently low at the stations on western Vancouver Island (BPBC, ETB, EDB, GDR, and OZB), possibly because the data for these stations are primarily earthquakes with epicenters near the Nootka fault zone and on the continental shelf or immediately inland (Zelt *et al.*, 1999). The Nootka fault zone is known to be a broad zone of fracturing separating the Juan de Fuca and Explorer plates (Hyndman and Rogers, 1981). Therefore, the low Q_0 here likely reflects the large sampled volume of highly fractured oceanic lithosphere, as well as the deformed accreted terranes along the west coast and beneath Vancouver Island (Havskov *et al.*, 1986; Zelt *et al.*, 1999). On a regional scale, this causes a contrast between south and north of the Vancouver Island with a drop of almost 10% of the estimated Q_0 on average at northern

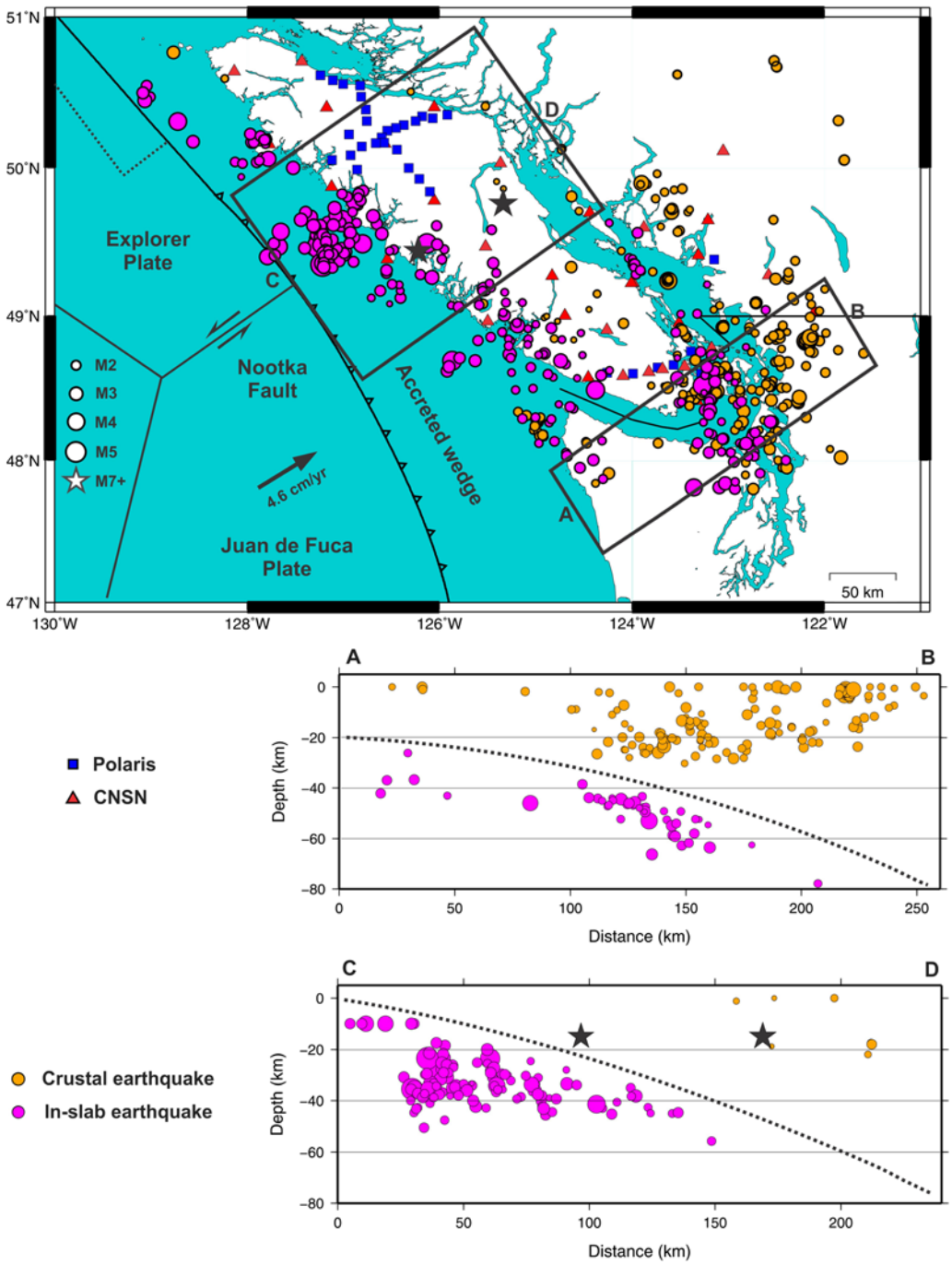

Figure 2. Selected earthquakes in the study area used for coda Q analysis. The dataset comprises 288 crustal earthquakes and 292 in-slab events recorded between 1985 and 2015. Event magnitudes range from 1.2 to 6.4. Depth distribution of earthquakes along A–B and C–D cross sections and subducting plate interface (black dotted line) are shown in the bottom. Black stars represent the locations of the only two known large ($\mathbf{M} \sim 7+$) crustal earthquakes on central Vancouver Island in the past 300 years. Depth of these two events is fixed at 15 km due to uncertainty of estimation. The color version of this figure is available only in the electronic edition.

Island stations ($Q_C = 68f^{0.94}$) including ETB, GDR, and CBB (Fig. 1) in comparison to the south ($Q_C = 76f^{0.87}$).

From the west coast of Vancouver Island, Q_0 increases to the east-southeast with the highest observed value of 121 ($a_2 = 100$ km) at station WPB and nearby stations (BIB, SHB, HNB, and VDB), all within the Coast belt. Another interesting observation is that stations (e.g., EDB, ETB, GDR, CBB, and NCRB) on west-central Vancouver Island closest to the landward projection of the Nootka fault zone and the location of the only two known large crustal earthquakes (1918, $\mathbf{M} \sim 7$ and 1946, $\mathbf{M} \sim 7.3$) on Vancouver Island have the lowest Q_0 values in our study area. For example, for $a_2 = 100$ km the only stations with $Q_0 < 75$ are these five stations mentioned above.

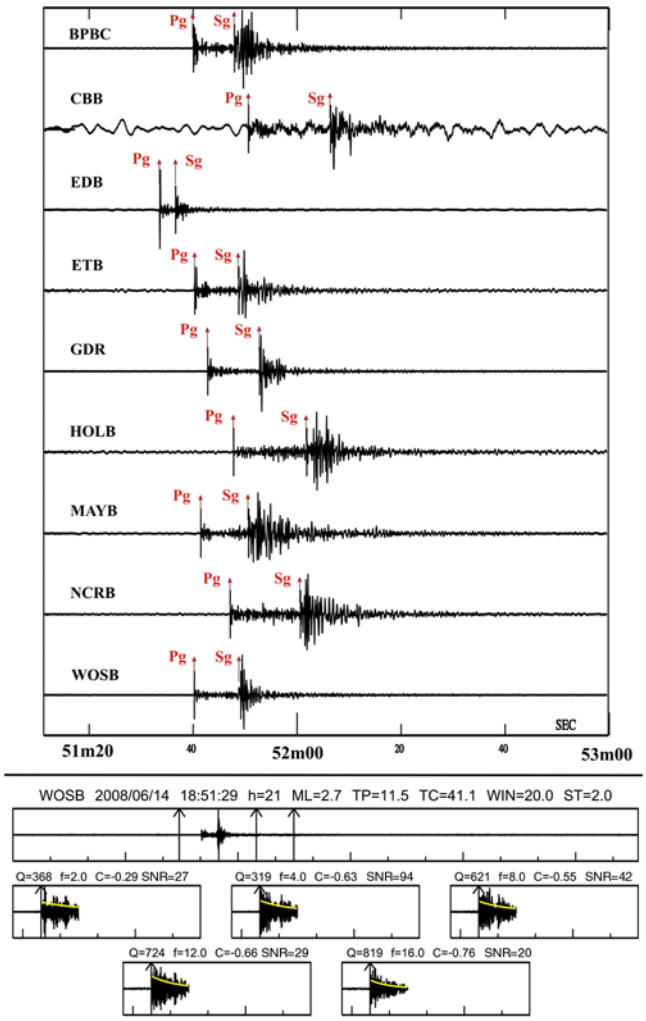

Figure 3. Data processing example for an earthquake beneath Vancouver Island recorded on 14 June 2008. The first step is a visual inspection of available waveforms (only vertical components are shown) and the selection of the closest stations to the event with the highest signal-to-noise ratio (top). In the bottom panel, the top trace is the original unfiltered waveform in which the three vertical lines indicate (from left) origin time, start, and end of coda window. Above the seismogram, station code, origin time, depth (h), magnitude (M_L), P-wave travel time (TP, s), start of coda window from the origin (TC, s), window length (WIN, s), and start of coda window in terms of S-wave travel time (t coda > ST, in which ST refers to ST $*$ $S-$travel time) are indicated. The amplitude decay corresponding to estimation parameters (f, frequency; C, correlation coefficient; SNR, signal-to-noise ratio) are shown by a curve in the five filtered segment. The color version of this figure is available only in the electronic edition.

Discussion and Conclusions

Resolution of crustal and upper-mantle attenuation models play an essential role in the accuracy of ground-motion estimates for seismic-hazard assessments (Pasyanos, 2011). Therefore, detailed investigation of attenuation parameters is necessary for each region. In this study, we conducted the most complete determination to date of coda Q in the northern Cascadia subduction zone (with a focus on southwestern British Columbia). We estimated Q_C for average lapse times between ~24 to ~60 s, corresponding to ellipse parameter a_2 of 40–100 km, respectively (a few trial estimates for an average lapse time of ~18 s/a_2 = 30 km are included in Ⓔ Table S3).

Based on previous studies, it has been shown that regional variation of seismic-wave attenuation can be related to the geotectonic setting of each region and the velocity structure (Carcolé and Sato, 2010). Our estimates of the coda Q values for the frequencies ranging between 2 to 16 Hz are evidently correlated with seismic activity and various tectonic settings. Comparing the distributions of Q_0 and α, an inverse correlation is observed over all the study area.

Our lowest Q_0 values were obtained in the western coastal range of Vancouver Island, whereas the highest Q_0 values for the region were observed in the Coast belt. Our results explicitly show lower attenuation and a lower decay rate in the stable regions (e.g., the Coast Mountains) compared with the more seismically active west coast of Vancouver Island. Stations on west-central Vancouver Island closest to the landward projection of the Nootka fault zone (e.g., EDB, ETB, GDR, CBB, and NCRB) and to the location of the only two known large crustal earthquakes (1918 **M** ~ 7 and 1946 **M** ~ 7.3) on Vancouver Island have the lowest Q_0 values in our study area, which creates a notable contrast in Q between north and south.

There are many reports of large earthquakes coincident with regions of low Q_0 (Jin and Aki, 1988). Attenuation studies in Japan, using high-resolution maps of coda Q, indicate that one of the regions of the lowest observed Q_C in the country, the Niigata-Kobe tectonic zone, has experienced large intraplate earthquakes including a magnitude 6.8 event on 23 October 2004 (Jin and Aki, 2005). It has been suggested that in this region the brittle-ductile transition zone is weakened by fluid from the upper mantle, which has increased the density of fluid-filled fractures in the ductile zone (Jin and Aki, 2005). Relationships between Q^{-1} and measures of earthquake rate have been attributed to aseismic creep in the brittle-ductile transition zone with characteristic fracture sizes (Jin and Aki, 1993). The long-term migration of coincident low Q_0 and high seismicity regions has also been attributed to a diffusion process associated with the aftershocks, fluid injection, and an inferred V_P/V_S anomaly (Jin and Aki, 1988).

In summary, an average frequency-dependent coda Q relationship $Q_C = 72f^{0.91}$ was obtained for southwestern British Columbia, whereas no significant difference was observed between the average Q_C for shallower (crustal) and deeper (in-slab) groups of earthquakes.

Our relation of frequency-dependent average coda Q represents a lower Q_0 and higher α than the corresponding previous estimates for southwestern British Columbia ($Q_C = 110f^{0.72}$; Zelt *et al.*, 1999) and higher Q_0 and lower α in comparison with results for northern Washington State ($Q_C = 63f^{0.97}$; Havskov *et al.*, 1989). Apart from the size of our database, which is much larger than those of the two pre-

Table 1
Average Q_0 and Estimated Uncertainties for Different Sampling Volumes

Station	$Q_0 \pm$ Error ($a_2 = 40$ km, $t_{lapse} = 24$ s)	$Q_0 \pm$ Error ($a_2 = 50$ km, $t_{lapse} = 30$ s)	$Q_0 \pm$ Error ($a_2 = 60$ km, $t_{lapse} = 36$ s)	$Q_0 \pm$ Error ($a_2 = 70$ km, $t_{lapse} = 42$ s)	$Q_0 \pm$ Error ($a_2 = 80$ km, $t_{lapse} = 48$ s)	$Q_0 \pm$ Error ($a_2 = 90$ km, $t_{lapse} = 54$ s)	$Q_0 \pm$ Error ($a_2 = 100$ km, $t_{lapse} = 60$ s)
ALB	-	67 ± 10(6)	82 ± 9(14)	68 ± 6(10)	73 ± 8(7)	76 ± 13(8)	85 ± 11(8)
BIB	72 ± 10(13)	82 ± 14(5)	79 ± 12(26)	86 ± 8(12)	84 ± 9(13)	100 ± 10(30)	112 ± 7(46)
BPBC	-	-	-	-	76 ± 12(6)	-	-
BTB	-	68 ± 9(9)	69 ± 5(10)	71 ± 11(9)	72 ± 10(14)	76 ± 9(15)	79 ± 7(54)
CBB	-	-	-	-	64 ± 4(6)	67 ± 8(8)	70 ± 6(24)
CLVB	-	-	73 ± 13(5)	-	-	80 ± 10(7)	-
EDB	61 ± 8(6)	63 ± 6(10)	66 ± 7(16)	69 ± 15(5)	65 ± 11(5)	67 ± 13(13)	72 ± 11(13)
ETB	54 ± 9(5)	44 ± 8(8)	53 ± 3(10)	-	58 ± 13(6)	66 ± 10(10)	-
GDR	-	-	71 ± 7(10)	78 ± 4(10)	65 ± 14(12)	76 ± 10(11)	75 ± 6(11)
GOBB	87 ± 9(10)	-	98 ± 12(25)	79 ± 9(13)	87 ± 10(8)	101 ± 11(21)	95 ± 12(9)
GOWB	94 ± 6(7)	-	105 ± 10(8)	-	-	108 ± 6(7)	-
HNB	-	-	102 ± 9(8)	100 ± 11(15)	105 ± 17(17)	118 ± 17(11)	113 ± 5(17)
HOLB	-	-	71 ± 8(7)	-	-	72 ± 9(5)	78 ± 10(10)
KELB	69 ± 12(6)	-	88 ± 9(9)	-	-	91 ± 16(8)	-
MAYB	-	-	-	-	-	-	96 ± 7(5)
MGB	-	70 ± 5(10)	66 ± 4(27)	67 ± 6(15)	98 ± 4(19)	91 ± 3(31)	85 ± 8(24)
MGCB	-	62 ± 13(6)	85 ± 12(10)	-	-	84 ± 17(8)	91 ± 9(3)
NAB	69 ± 8(5)	-	78 ± 17(14)	74 ± 16(6)	77 ± 14(6)	97 ± 6(24)	90 ± 4(14)
NCRB	-	-	-	-	-	68 ± 10(7)	71 ± 8(10)
NLLB	-	-	92 ± 7(5)	-	-	90 ± 4(5)	95 ± 3(8)
OZB	71 ± 7(11)	70 ± 10(10)	69 ± 11(10)	74 ± 12(7)	90 ± 10(9)	87 ± 14(8)	82 ± 11(10)
PFB	70 ± 12(5)	-	71 ± 5(7)	72 ± 6(6)	81 ± 10(7)	96 ± 7(13)	91 ± 9(16)
PGC	-	79 ± 13(6)	87 ± 6(18)	86 ± 5(10)	95 ± 12(14)	98 ± 14(13)	100 ± 8(10)
PHC	-	-	63 ± 11(5)	-	-	-	-
SHB	-	-	101 ± 15(6)	-	-	117 ± 6(7)	110 ± 4(19)
SILB	-	56 ± 7(6)	66 ± 12(10)	-	-	91 ± 20(8)	83 ± 8(6)
SNB	-	107 ± 5(6)	109 ± 7(17)	100 ± 9(9)	105 ± 6(11)	110 ± 4(16)	112 ± 6(14)
SSIB	-	-	86 ± 17(10)	-	-	97 ± 10(5)	-
TSJB	-	-	70 ± 14(5)	-	-	80 ± 6(9)	81 ± 9(5)
TWBB	-	-	69 ± 15(7)	-	77 ± 7(8)	80 ± 5(15)	89 ± 11(7)
TWGB	-	-	72 ± 15(5)	-	76 ± 4(5)	76 ± 4(5)	-
TWKB	-	-	70 ± 18(7)	72 ± 8(5)	-	88 ± 20(6)	89 ± 10(5)
TXB	-	-	89 ± 8(9)	-	107 ± 11(6)	100 ± 9(14)	108 ± 7(26)
VDB	66 ± 9(6)	-	80 ± 12(11)	97 ± 15(10)	102 ± 13(15)	104 ± 9(17)	107 ± 10(15)
VGZ	65 ± 16(10)	65 ± 11(20)	73 ± 9(38)	74 ± 10(15)	82 ± 8(16)	100 ± 6(25)	103 ± 9(16)
VI05	-	-	-	79 ± 12(5)	-	-	-
VI08	-	-	72 ± 11(6)	-	-	-	-
VI52	-	-	-	78 ± 14(5)	-	-	-
WOSB	-	-	73 ± 12(5)	-	77 ± 14(6)	84 ± 12(14)	89 ± 15(6)
WPB	-	-	92 ± 10(17)	101 ± 12(8)	107 ± 11(19)	118 ± 13(26)	121 ± 10(47)
YOUB	-	-	-	73 ± 8(6)	77 ± 12(6)	84 ± 18(8)	76 ± 16(5)

Number of events is given in parentheses after each estimated value ($n \geq 5$).

vious studies combined together, we used a larger range of appropriate lapse times to compute our estimates.

In comparison with the previous study (Zelt *et al.*, 1999) in southwestern British Columbia, we significantly increased the resolution of the estimates of Q_C by reducing the minimum average lapse time from 36 s ($a_2 = 60$ km) to 24 s ($a_2 = 40$ km). Therefore, events with shorter lapse times and smaller Q_C values make a larger contribution to our final average Q_C estimate. Some results from Washington state (Havskov *et al.*, 1989) are also influenced by very shallow volcanic-induced earthquakes near Mount St. Helens (with typically very low Q_C) and used source–station distances that were limited to ~70 km, compared with the upper limit of ~110 km in our study.

Increase of Q_C with lapse time arises from the average attenuation properties of the crust and upper mantle at different depths. Deviations from this general trend are mainly due to site effects, which may dominate the early coda in regions with resonant structures such as sedimentary basins (Steck *et al.*, 1989) and local anomalies such as low-velocity zones within subducting plate in the Cascadia subduction zone (Audet *et al.*, 2009; Hansen *et al.*, 2012).

Our study has clearly defined variations in coda Q across the northern Cascadia subduction zone, with higher attenuation (low Q) in the seismically active areas of Vancouver Island (and near the largest historic earthquakes) and lower attenuation (highest Q) in the seismically quiescent Coast Mountains region further inland. As additional

Table 2
Average α Values and Estimated Uncertainties and Average Z_{max} for Different Sampling Volumes ($n \geq 5$)

Station	$\alpha \pm$ Error ($a_2 = 40$ km, $t_{lapse} = 24$ s)	$\alpha \pm$ Error ($a_2 = 50$ km, $t_{lapse} = 30$ s)	$\alpha \pm$ Error ($a_2 = 60$ km, $t_{lapse} = 36$ s)	$\alpha \pm$ Error ($a_2 = 70$ km, $t_{lapse} = 40$ s)	$\alpha \pm$ Error ($a_2 = 80$ km, $t_{lapse} = 48$ s)	$\alpha \pm$ Error ($a_2 = 90$ km, $t_{lapse} = 54$ s)	$\alpha \pm$ Error ($a_2 = 100$ km, $t_{lapse} = 60$ s)
ALB	-	0.96 ± 0.05	0.87 ± 0.04	0.95 ± 0.03	0.98 ± 0.05	0.88 ± 0.08	0.86 ± 0.10
BIB	0.90 ± 0.06	0.78 ± 0.06	0.79 ± 0.07	0.82 ± 0.04	0.81 ± 0.03	0.79 ± 0.04	0.73 ± 0.03
BPBC	-	-	-	-	0.87 ± 0.09	-	-
BTB	-	0.93 ± 0.06	0.89 ± 0.04	0.96 ± 0.08	0.93 ± 0.07	0.93 ± 0.06	0.88 ± 0.04
CBB	-	-	-	-	0.94 ± 0.01	0.96 ± 0.04	0.97 ± 0.04
CLVB	-	-	0.78 ± 0.06	-	-	0.83 ± 0.02	-
EDB	0.87 ± 0.06	0.85 ± 0.03	0.96 ± 0.06	0.95 ± 0.12	0.96 ± 0.12	1.00 ± 0.13	0.95 ± 0.11
ETB	0.96 ± 0.06	1.09 ± 0.05	1.09 ± 0.05	-	0.92 ± 0.12	0.77 ± 0.06	-
GDR	-	-	0.94 ± 0.05	0.88 ± 0.02	0.98 ± 0.09	0.89 ± 0.07	0.93 ± 0.04
GOBB	0.78 ± 0.05	-	0.77 ± 0.03	0.82 ± 0.05	0.91 ± 0.06	0.69 ± 0.01	0.82 ± 0.06
GOWB	0.77 ± 0.01	-	0.70 ± 0.01	-	-	0.80 ± 0.05	-
HNB	-	-	0.75 ± 0.04	0.75 ± 0.08	0.73 ± 0.15	0.74 ± 0.11	0.65 ± 0.01
HOLB	-	-	0.95 ± 0.08	-	-	0.81 ± 0.16	0.87 ± 0.07
KELB	0.85 ± 0.11	-	0.77 ± 0.02	-	-	0.82 ± 0.16	-
MAYB	-	-	-	-	-	-	0.84 ± 0.07
MGB	-	0.95 ± 0.04	0.93 ± 0.01	0.94 ± 0.05	0.79 ± 0.03	0.80 ± 0.02	0.87 ± 0.05
MGCB	-	0.92 ± 0.12	0.75 ± 0.07	-	-	0.87 ± 0.11	0.79 ± 0.08
NAB	0.80 ± 0.04	-	0.81 ± 0.12	0.83 ± 0.12	0.83 ± 0.12	0.73 ± 0.04	0.80 ± 0.01
NCRB	-	-	-	-	-	0.94 ± 0.04	0.97 ± 0.06
NLLB	-	-	0.75 ± 0.06	-	-	0.80 ± 0.03	0.79 ± 0.04
OZB	0.85 ± 0.06	0.92 ± 0.08	0.94 ± 0.88	0.98 ± 0.08	0.88 ± 0.11	0.71 ± 0.02	0.96 ± 0.06
PFB	0.91 ± 0.09	-	0.92 ± 0.01	0.94 ± 0.03	0.86 ± 0.06	0.83 ± 0.03	0.85 ± 0.04
PGC	-	0.79 ± 0.13	0.76 ± 0.02	0.78 ± 0.04	0.86 ± 0.09	0.78 ± 0.12	0.81 ± 0.08
PHC	-	-	1.00 ± 0.09	-	-	-	-
SHB	-	-	0.76 ± 0.13	-	-	0.71 ± 0.04	0.77 ± 0.02
SILB	-	0.95 ± 0.06	0.85 ± 0.03	-	-	0.78 ± 0.15	0.80 ± 0.05
SNB	-	0.72 ± 0.04	0.68 ± 0.05	0.69 ± 0.06	0.74 ± 0.03	0.71 ± 0.01	0.72 ± 0.05
SSIB	-	-	0.79 ± 0.11	-	-	0.73 ± 0.03	-
TSJB	-	-	0.92 ± 0.06	-	-	0.83 ± 0.05	0.84 ± 0.04
TWBB	-	-	0.89 ± 0.07	-	0.85 ± 0.04	0.85 ± 0.04	0.78 ± 0.09
TWGB	-	-	0.84 ± 0.08	-	0.87 ± 0.02	0.87 ± 0.03	-
TWKB	-	-	0.92 ± 0.13	0.91 ± 0.07	-	0.73 ± 0.15	0.81 ± 0.06
	-	-	0.77 ± 0.04	-	0.68 ± 0.08	0.77 ± 0.03	0.74 ± 0.04
TXB	0.83 ± 0.02	-	0.74 ± 0.11	0.79 ± 0.11	0.74 ± 0.11	0.72 ± 0.07	0.75 ± 0.05
VDB	0.87 ± 0.09	0.87 ± 0.07	0.88 ± 0.05	0.91 ± 0.05	0.83 ± 0.02	0.76 ± 0.03	0.75 ± 0.02
VGZ	-	-	-	0.85 ± 0.06	-	-	-
VI05	-	-	0.89 ± 0.07	-	-	-	-
VI08	-	-	-	0.88 ± 0.04	-	-	-
VI52	-	-	0.86 ± 0.07	-	0.90 ± 0.15	0.86 ± 0.08	0.77 ± 0.10
WOSB	-	-	0.79 ± 0.03	0.74 ± 0.04	0.73 ± 0.04	0.69 ± 0.04	0.67 ± 0.02
WPB	-	-	-	0.74 ± 0.04	0.89 ± 0.08	0.85 ± 0.11	0.89 ± 0.01
YOUB							
Average Z_{max}	50 ± 6 km	64 ± 4 km	74 ± 5 km	85 ± 7 km	94 ± 6 km	104 ± 7 km	112 ± 5 km

seismic data are collected in this region we expect that additional low lapse-time recordings will allow for near-site geological conditions and local site effects on coda Q to be better constrained.

Data and Resources

Seismograms used in this study were downloaded from the archive of the Canadian National Seismographic Network (CNSN) and Portable Observatories for Lithospheric Analysis and Research Investigating Seismicity (POLARIS) networks. Waveform data can be obtained from CNSN Data Centre using www.earthquakescanada.nrcan.gc.ca/stndon/NWFA-ANFO/index-eng.php (last accessed April 2015). The software SEISAN and user manual can be obtained at http://seisan.info (last accessed July 2012). Some plots were made using the Generic Mapping Tools v.4.2.1 (www.soest.hawaii.edu/gmt, last accessed May 2014). The unpublished data by A. M. Farahbod and A. J. Calvert (2007), "Location of non-volcanic tremors along the Cascadia subduction zone", is available from the U.S. Geological Survey at http://earthquake.usgs.gov/research/external/research.php?yearID=2006&regionID=7&submit=Find+Projects (last accessed February 2008).

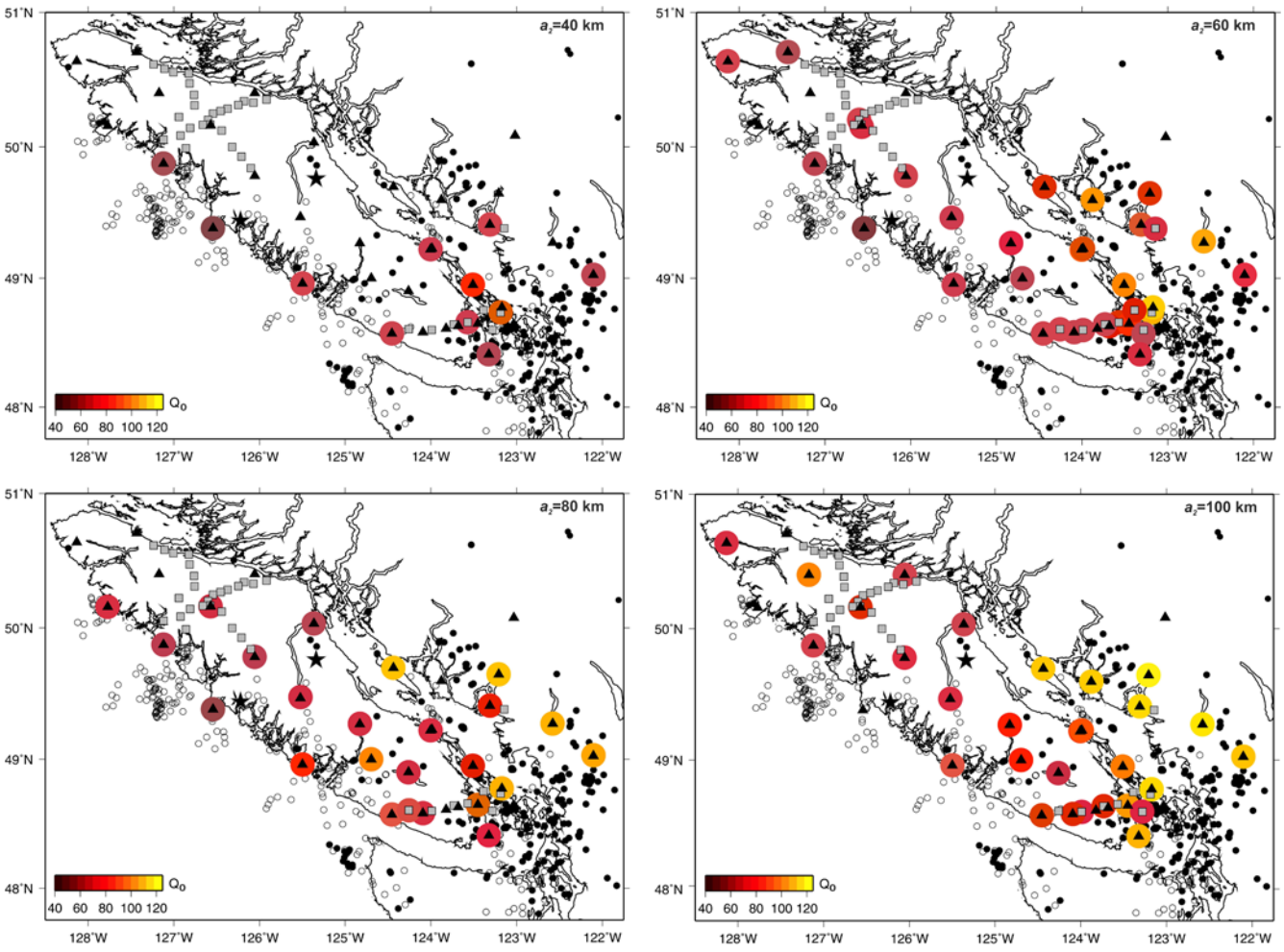

Figure 4. Map of Q_0 variations in southwestern British Columbia with ellipse parameter a_2 between 40 km (top left) and 100 km (bottom right). Only stations with five or more events are shown. Triangles indicate CNSN broadband and short-period stations. Squares are POLARIS broadband seismograph stations. Stars represent the locations of the only two known large crustal earthquakes on central Vancouver Island in the past 300 yrs. The color version of this figure is available only in the electronic edition.

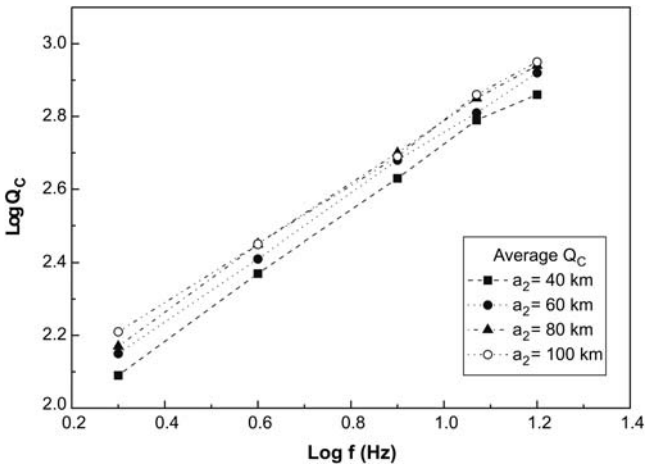

Figure 5. Logarithmic plots of the overall average variation of coda Q with frequency and ellipse parameters between $a_2 = 40$ km and $a_2 = 100$ km.

Acknowledgments

We thank Jens Havskov and Taimi Mulder and two anonymous reviewers for their thorough reviews and constructive criticism, which greatly improved the article. We would also like to acknowledge the Canadian National Seismographic Network (CNSN) and Portable Observatories for Lithospheric Analysis and Research Investigating Seismicity (POLARIS) networks, from which the seismic data were obtained. This study was partly funded by the Natural Sciences and Engineering Council of Canada. This is Earth Sciences Sector (ESS) Contribution Number 20160082.

References

Aki, K. (1969). Analysis of the seismic coda of local earthquakes as scattered waves, *J. Geophys. Res.* **74,** 615–631.

Aki, K., and B. Chouet (1975). Origin of coda waves: Source, attenuation, and scattering effects, *J. Geophys. Res.* **80,** 3322–3342.

Audet, P., M. G. Bostock, N. I. Christensen, and S. M. Peacock (2009). Seismic evidence for overpressured subducted oceanic crust and megathrust fault sealing, *Nature* **457,** 76–78.

Carcolé, E., and H. Sato (2010). Spatial distribution of scattering loss and intrinsic absorption of short-period *S* waves in the lithosphere of

Japan on the basis of the multiple lapse time window analysis of Hi-net data, *Geophys. J. Int.* **180,** 268–290, doi: 10.1111/j.1365-246X.2009.04394.x.

Gusev, A. A. (1995). Vertical profile of turbidity and coda Q, *Geophys. J. Int.* **123,** 665–672.

Hansen, R. T. J., M. G. Bostock, and N. I. Christensen (2012). Nature of the low velocity zone in Cascadia from receiver function waveform inversion, *Earth Planet. Sci. Lett.* **337/338,** 25–38, doi: 10.1016/j.epsl.2012.05.031.

Havskov, J., and L. Ottemöller (2010). *Routine Data Processing in Earthquake Seismology*, Springer, Berlin, Germany, 347 pp., ISBN: 978-90-481-8696-9.

Havskov, J., and L. Ottemöller (2012). *SEISAN: The Earthquake Analysis Software*, v. 8.2.1, Department of Earth Science, University of Bergen, Bergen, Norway.

Havskov, J., L. Kvamme, and H. Bungum (1986). Attenuation of seismic waves in the Jan Mayen Island area, *Mar. Geophys. Res.* **8,** 39–47.

Havskov, J., S. Malone, D. McClurg, and R. Crosson (1989). Coda Q for the state of Washington, *Bull. Seismol. Soc. Am.* **79,** no. 4, 1024–1038.

Havskov, J., M. B. Sørensen, D. Vales, M. Özyazıcıoğlu, G. Sánchez, and B. Li (2016). Coda Q in different tectonic areas, influence of processing parameters, *Bull. Seismol. Soc. Am.* **106,** no. 3, 956–970, doi: 10.1785/0120150359.

Hyndman, R. D., and G. C. Rogers (1981). Seismicity surveys with ocean bottom seismographs off western Canada, *J. Geophys. Res.* **86,** 3867–3880.

Jin, A., and K. Aki (1988). Spatial and temporal correlation between coda Q and seismicity in China, *Bull. Seismol. Soc. Am.* **78,** 741–769.

Jin, A., and K. Aki (1989). Spatial and temporal correlation between coda Q^{-1} and seismicity and its physical mechanism, *J. Geophys. Res.* **94,** 14,041–14,059.

Jin, A., and K. Aki (1993). Temporal correlation between coda Q^{-1} and seismicity—Evidence for a structural unit in the brittle-ductile transition zone, *J. Geodyn.* **17,** no. 3, 95–119.

Jin, A., and K. Aki (2005). High-resolution maps of coda Q in Japan and their interpretation by the brittle-ductile interaction hypothesis, *Earth Planets Space* **57,** 403–409.

Mak, S., L. S. Chan, A. M. Chandler, and R. C. H. Koo (2004). Coda Q estimates in the Hong Kong Region, *J. Asian Earth Sci.* **24,** 127–136.

Mitchell, B. J., and L. Cong (1998). *Lg* coda Q and its relation to the structure and evolution of continents: A global perspective, *Pure Appl. Geophys.* **153,** 655–663.

Monger, J., and R. Price (2002). The Canadian Cordillera: Geology and tectonic evolution, *CSEG Recorder* **27,** no. 2, 17–36.

Pasyanos, M. E. (2011). A case for the use of 3D attenuation models in ground motion and seismic hazard assessment, *Bull. Seismol. Soc. Am.* **101,** 1965–1970, doi: 10.1785/0120110004.

Pauli, J. J. (1984). Attenuation of coda waves in New England, *Bull. Seismol. Soc. Am.* **74,** 1149–1166.

Rautian, T. G., and V. I. Khalturin (1978). The use of the coda for determination of the earthquake source spectrum, *Bull. Seismol. Soc. Am.* **68,** 923–948.

Sato, H. (1977). Energy propagation including scattering effects: Single isotropic scattering approximation, *J. Phys. Earth* **25,** 27–41.

Sato, H., and M. C. Fehler (1998). *Seismic Wave Propagation and Scattering in the Heterogeneous Earth*, Springer-Verlag, New York, New York, 308 pp.

Steck, L. K., W. A. Prothero, and J. Scheimer (1989). Site-dependent coda Q at Mono Craters, California, *Bull. Seismol. Soc. Am.* **79,** 1559–1574.

Wu, R. S., and K. Aki (1988). Multiple scattering and energy transfer of seismic waves: Separation of scattering effect from intrinsic attenuation. II. Application of the theory to Hindu Kush region, *Pure Appl. Geophys.* 128**,** 49–80.

Zelt, B. C., N. T. Dotzev, R. M. Ellis, and G. C. Rogers (1999). Coda Q in southwestern British Columbia, Canada, *Bull. Seismol. Soc. Am.* **89,** no. 4, 1083–1093.

Pacific Geoscience Centre
Geological Survey of Canada
Natural Resources Canada
9860 West Saanich Road
Sidney, British Columbia
Canada V8L 4B2
(A.M.F., J.F.C., C.B.)

Simon Fraser University
Department of Earth Sciences
8888 University Drive
Burnaby, British Columbia
Canada V5A 1S6
(A.J.C.)

Manuscript received 23 February 2016;
Published Online 23 August 2016